REPORT DOCUMENTATION PAGE

Form Approved
OBM No. 0704-0188

AD-A257 929

timated to average 1 hour per response, including the time for reviewing instructions, searching existing data sources, gathering and s collection of information. Send comments regarding this burden or any other aspect of this collection of information, including suggestions es, Directorate for Information Operations and Reports, 1215 Jefferson Davis Highway, Suite 1204, Arlington, VA 22202-4302, and to n Project (0704-0188), Washington, DC 20503.

Report Date.	3. Report Type and Dates Covered.
October 1992	Final - Journal Article

Source imaging and sidelobe suppression using time-domain techniques in a shallow-water waveguide

5. Funding Numbers.

Contract	
Program Element No.	0601153N
Project No.	03202
Task No.	350
Accession No.	DN255005
Work Unit No.	12442B

6. Author(s).
C. Feuillade and C. S. Clay*

7. Performing Organization Name(s) and Address(es).
Naval Oceanographic and Atmospheric Research Laboratory
Ocean Acoustics and Technology Directorate
Stennis Space Center, MS 39529-5004

DTIC ELECTE NOV23 1992 S E D

8. Performing Organization Report Number.
JA 243:034:92

9. Sponsoring/Monitoring Agency Name(s) and Address(es).
Naval Oceanographic and Atmospheric Research Laboratory
Basic Research and Management Office
Stennis Space Center, MS 39529-5004

10. Sponsoring/Monitoring Agency Report Number.
JA 243:034:92

11. Supplementary Notes.
*Geophysical and Polar Research Center, University of Wisconsin-Madison, 1215 West Dayton Street, Madison, Wisconsin 53706
Published in J. Acoust. Soc. Am.

12a. Distribution/Availability Statement.
Approved for public release; distribution is unlimited.

12b. Distribution Code.

13. Abstract *(Maximum 200 words).*

Source localization in a shallow-water waveguide, using harmonic (cw) techniques, is typically complicated by the repetitive sidelobe structure of the acoustic field. For this reason, much interest has been shown recently in the development and implementation of time-domain methods, which should achieve better performance because of their additional frequency-averaging capability. In a previous publication [C. S. Clay, J. Acoust. Soc. Am. 81, 660-664 (1987)], the basis for optimum signal transmission and source localization in a waveguide using time-domain techniques was described. In this present work a simple two-layer Pekeris model with shallow water depth (20 m) and short range (1500 m) has been used to compute image resolution and sidelobe suppression as a function of frequency bandwidth, number of modes, and the number of receivers in an array. The results indicate that source localization performance is most strongly dependent upon the bandwidth and number of modes available to carry the signal transmission. The physical mechanism for narrowing the source image and suppressing sidelobes is spatial averaging of the acoustic field due to variation of the horizontal wave numbers for the modes as a function of frequency. Improvements in mode sampling, by increasing the number of receivers, also reduced the level of sidelobes, but did not improve the resolution of the image.

14. Subject Terms.
Shallow-water, algorithms, matched-field

15. Number of Pages.
8

16. Price Code.

17. Security Classification of Report.	18. Security Classification of This Page.	19. Security Classification of Abstract.	20. Limitation of Abstract.
Unclassified	Unclassified	Unclassified	SAR

Source imaging and sidelobe suppression using time-domain techniques in a shallow-water waveguide

C. Feuillade
Naval Research Laboratory, Stennis Space Center, Mississippi 39529-5004

C. S. Clay
Geophysical and Polar Research Center, University of Wisconsin–Madison, 1215 West Dayton Street, Madison, Wisconsin 53706

(Received 18 February 1992; accepted for publication 22 June 1992)

92-29966

Source localization in a shallow-water waveguide, using harmonic (cw) techniques, is typically complicated by the repetitive sidelobe structure of the acoustic field. For this reason, much interest has been shown recently in the development and implementation of time-domain methods, which should achieve better performance because of their additional frequency-averaging capability. In a previous publication [C. S. Clay, J. Acoust. Soc. Am. **81**, 660–664 (1987)], the basis for optimum signal transmission and source localization in a waveguide using time-domain techniques was described. In this present work a simple two-layer Pekeris model with shallow water depth (20 m) and short range (1500 m) has been used to compute image resolution and sidelobe suppression as a function of frequency bandwidth, number of modes, and the number of receivers in an array. The results indicate that source localization performance is most strongly dependent upon the bandwidth and number of modes available to carry the signal transmission. The physical mechanism for narrowing the source image and suppressing sidelobes is spatial averaging of the acoustic field due to variation of the horizontal wave numbers for the modes as a function of frequency. Improvements in mode sampling, by increasing the number of receivers, also reduced the level of sidelobes, but did not improve the resolution of the image.

PACS numbers: 43.30.Wi, 43.20.Mv

INTRODUCTION

In a series of recent papers, Clay[1-3] has described the use of matched filters and deconvolving filters to locate a transient (or impulsive) source in a waveguide. His technique uses the transmission from the source along the waveguide to one or two receivers. A matched filter is applied to the received signal which, by reciprocity, is equivalent to the transmission of the time-reversed signal from the receiver back to the source position. A mapping of the field in the waveguide gives the source location. Both the numerical studies and experiments showed that false locations and sidelobe ambiguities are serious problems. To improve resolution, the next logical step is to receive an impulsive transmission at an array of receivers and use more channels of information. The ensemble of time-reversed signals from the array then constitutes an impulse hologram.[4] If one projects the time reversal of the signals from the array, one gets an image of the source in the backward direction. Projection of the impulse hologram in the forward direction continues the propagation in the waveguide.

Source imaging using impulse or time-domain holography is related to conventional matched-array filtering or matched-field source location techniques.[5,6] Impulse holography uses many frequencies and one or two receivers while matched-field techniques use one frequency and many receivers. In a sense they are related by Fourier transformations. It seems reasonable to expect that the combination of many frequencies and receiving arrays ought to work better than either technique alone. One of our purposes here is to explore the dependence of location performance of impulse holography on the number of receivers in an array.

Impulse holography uses the actual data set recorded at an array of hydrophones to reconstruct the wave fronts, and therefore the imaging operation does not require prior assumptions about the number and nature of the sources. The source emissions can include impulsive, random, and periodic sources. However, the acoustical properties and characteristics of the waveguide must be known. The capability to perform the appropriate acoustic propagation computations is also required. Time-domain imaging of this type is closely related to seismic imaging methods, and is known as migration in the literature of exploration geophysics.[4,7]

Clearly, the resolution of the source in the waveguide, and the degree of sidelobe contamination, will strongly depend on the acoustic environment and the waveguide structure. The more complex the waveguide environment is, the more uniquely a specific location within it may be defined. This uniqueness will generally improve the resolution of the source and reduce the ambiguities due to sidelobes. However, the increased complexity of the waveguide also makes it more difficult to isolate and analyze the effects of individual waveguide parameters on the matched-filtering process. In order to better understand the nature and variability of this process we decided to adopt a simple waveguide model, so that we could investigate the optimum filter as a function

 © 1992 Acoustical Society of America

of only a few parameters. Problems in source identification and location due to increased sidelobes were avoided by careful choice of the search procedure, which we shall describe later. In the work reported here, therefore, the variation in time-domain image resolution and sidelobe reduction as a function of frequency bandwidth, mode selection, and the number of hydrophone receivers, are investigated for a simple two-layer Pekeris waveguide model with shallow water depth (20 m) and short range (1500 m). The range of acoustic frequencies limited the number of normal modes propagating through the waveguide to the first 13 modes.

Section I of this paper gives a brief review of the propagation theory and correlation technique used in this study. Section II gives signal transmissions. Section III gives a locator and measure of performance. Section IV discusses the effects on the performance of the time-domain matched-filter technique of varying the bandwidth, mode, and number of receivers. This is followed by a summary of the conclusions drawn from the study.

I. THEORY

The normal mode formulation of the transmission problem was chosen because a set of eigenfunctions for each frequency is sufficient to compute the pressure fields everywhere. We believed that the numerical cost of making mode calculations at many frequencies would be lower than the cost of making ray traces to many receivers. Actually the computation times were larger than we expected. Even though it was necessary to compute the eigenfunctions only once, the subsequent calculation of the pressure fields still proved costly because closely spaced frequencies were required to avoid difficulties due to "wrap around" effects in the Fourier transformation process.

Referring to Fig. 1, we follow the procedure outlined in the introduction by first propagating a transient signal from the source to one or more receivers on the vertical hydrophone array; and then matched-filtering the received signals by time-reversing them and propagating them back along the waveguide to the source location (or to positions *adjacent* to the source location). We will compare these re-transmitted signals, with that re-transmitted and received at the correct source location, as a function of range mismatch only (i.e., we use the correct source depth for all calculations). This assumption simplifies the study considerably and facilitates the purpose of isolating and identifying the effects of varying the relevant parameters on the filtering process.

The source spectrum $S(\omega)$ and the transmission function to the nth receiver $T_n(r_{sn},\omega)$ are written separately, where ω is the angular frequency $2\pi f$. For simplicity, we start with the transmission to one receiver and then extend the derivation to N receivers. The transmission function has the usual normal mode solution for a harmonic source[5,8,9]

$$T_n(r_{sn},\omega) = \sum_m \phi_m(z_s)\phi_m(z_n)U_m(r_{sn}), \tag{1}$$

where z_s and z_n are suppressed in the notation for T_n but are implied by the argument r_{sn}, and

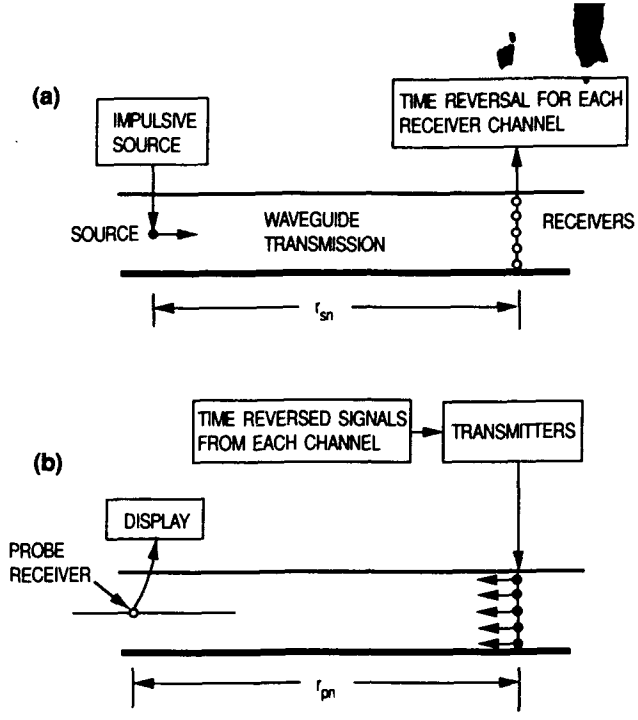

FIG. 1. Transmissions in a waveguide. (a) An impulse is transmitted from the source and received at an array of receivers. The signal from each receiver is time reversed and stored for later transmission. The receivers are numbered from 1 to N and are at the depths z_n. (b) The time-reversed signals are transmitted by transducers at the same locations as the receivers.

$$U_m(r_{sn}) = (q_m/\sqrt{r_{sn}})e^{-i\kappa_m r_{sn}}, \tag{2}$$

κ_m = horizontal component of the wave number,

r_{sn} = range from source to nth receiver,

q_m = excitation function, (3)

$\phi_m(z)$ = eigenfunction for source or receiver,

z_s = source depth, and z_n = receiver depth.

Letting $S(\omega)$ be the Fourier transformation of the source signal $s(t)$, the spectral amplitude of the pressure signal at the nth receiver is

$$P_n(r_{sn},\omega) = S(\omega)T_n(r_{sn},\omega), \tag{4}$$

and the pressure signal is

$$p_n(r_{sn},t) = \int_{-\infty}^{\infty} P_n(r_{sn},\omega)e^{i2\pi ft}\,df. \tag{5}$$

In the work described here the source spectrum $S(\omega)$ is a boxcar function of variable bandwidth. The Fourier transformation of this function gives a transmitted time signal $s(t)$ with a sinc function envelope.

A. Time-reversed signal

The complex conjugate of (5) gives the time reversed or matched signal

$$p_n(r_{sn}, t) = \int_{-\infty}^{\infty} P_n^*(r_{sn},\omega)e^{-i2\pi ft}\,df. \tag{6}$$

The holographic image is formed by transmitting the time-reversed signal through the transmission function. The image is mapped by numerically transmitting the time-reversed signal to "probe receivers" at a set of ranges and

depths, r_{pn} and z_p. In our numerical examples, the probe depth was chosen to be the same as the source depth so that we could concentrate on the range effects. The spectral amplitude of the pressure at the probe position is

$$P_p(r_{pn},\omega) = P_n^*(r_{sn},\omega)T_n(r_{pn},\omega), \tag{7}$$

$$P_p(r_{pn},\omega) = S^*(\omega)T_n^*(r_{sn},\omega)T_n(r_{pn},\omega). \tag{8}$$

The substitution of the mode summations (1) gives a double summation where we use m and m' as the summation indices:

$$P_p(r_{pn},\omega) = S^*(\omega)\sum_m\sum_{m'}\phi_m^*(z_s)\phi_m^*(z_n)\phi_{m'}(z_p) \times\phi_{m'}(z_n)U_m^*(r_{sn})U_{m'}(r_{pn}). \tag{9}$$

The range information is carried in the product

$$U_m^*(r_{sn})U_{m'}(r_{pn}) = \frac{q_m q_{m'}}{(r_{sn}r_{pn})^{1/2}}\exp[i(\kappa_m r_{sn} - \kappa_{m'} r_{pn})], \tag{10}$$

and the depth information is carried in the product of the eigenfunctions, the $\phi_m(z_s)$, etc. We note that, since the U and ϕ functions appear together within the double summation in (9), the range and depth information about the source does not appear to be simply separable except by filtering individual modes.

The time domain pressure $p_p(r_{pn},t)$ is the Fourier transformation of the spectrum

$$p_p(r_{pn},t) = \int_{-\infty}^{\infty} P_p(r_{pn},\omega)e^{i2\pi ft}\,df. \tag{11}$$

The expressions are evaluated numerically by using a finite or discrete Fourier transformation algorithm.

While the original pressure $p(r_{pn},t)$ may be a transient function of time, the finite Fourier transformations do a "wrap around" and "create" a periodic function

$$p(r_{pn},t) = p(r_{pn},t+T), \tag{12}$$

where T is the fundamental period of the Fourier transformation. Since the transmission is dispersive and the group velocities decrease with increasing mode number, some preliminary computations are needed to estimate signal travel times and durations. Commonly the fundamental period T is chosen to be roughly twice the duration of the signal.

B. Array of receivers

The computations of $p(r_{pn},t)$ are repeated for each receiver and then summed over the array of N receivers to give a "pixel" of an image at r_p and z_p

$$s_p(t) = \sum_{n=1}^{N} p_p(r_{pn},t) \tag{13}$$

and the substitution of the summation and Fourier transformation gives

$$s_p(t) = \int_{-\infty}^{\infty} S^*(\omega)\sum_{n=1}^{N} T_n^*(r_{sn},\omega)T_n(r_{pn},\omega)e^{i2\pi ft}\,df. \tag{14}$$

We note that the image function $s_p(t)$ is the convolution of the source spectrum $S(\omega)$ with the cross correlation of $T_n(r_{sn},\omega)$ and $T_n(r_{pn},\omega)$, summed over receivers. In our following discussion we will use the term "correlation peak" to mean the peak of the cross correlation of $T_n(r_{sn},\omega)$ and $T_n(r_{pn},\omega)$. The Fourier integral can be replaced by the finite Fourier summation by letting T be the duration of the signal and J be the number of samples. The sampling interval and frequencies are

$$\Delta t = T/J \text{ and } t_k = k\,\Delta t, \tag{15}$$

$$\omega_j = 2\pi j/T. \tag{16}$$

The equivalent summation for the finite Fourier series is

$$s_p(k\,\Delta t) = \sum_{j=0}^{J-1}\sum_{n=1}^{N} S\left(2\pi\frac{j}{T}\right)T_n^*\left(r_{sn},2\pi\frac{j}{T}\right)T_n\left(r_{pn},2\pi\frac{j}{T}\right) \times\exp\left(i2\pi\frac{jk\,\Delta t}{T}\right), \tag{17}$$

where again T is the fundamental period.

II. SIGNAL TRANSMISSIONS

The geoacoustic environmental model used for this study is the two-layered liquid half-space model of Pekeris.[10] The model consists of a shallow isospeed water layer of uniform density overlying a faster, isospeed, semi-infinite fluid bottom of uniform (and usually higher) density. The Pekeris model is a widely used, well-understood standard model; and even though it is a simple model it does possess features that are very similar to several matched-field experiments that have been performed. Since the acoustic wave functions within the waveguide are calculated analytically, without need for recourse to numerical techniques, the performance of the propagation calculations for the study is greatly facilitated. Thus, the two-layer Pekeris model is a good choice for present purposes. The parameters are given in Fig. 2. No acoustic attenuation is included for either layer. The acoustic frequencies used vary from 54 to 878.5 Hz. In this waveguide, this frequency range gives rise to a minimum of 1 mode and a maximum of 13 modes. The transmitted source spectrum is a boxcar function. The lower frequency

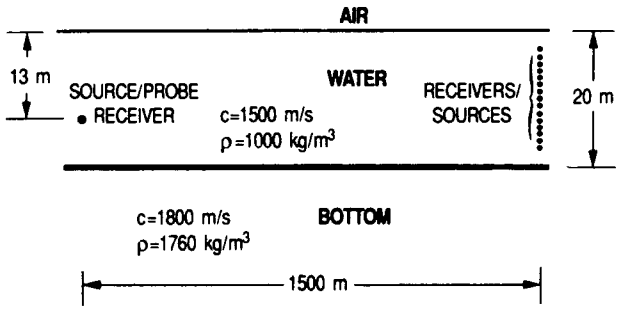

FIG. 2. Waveguide geometry and parameters. The uniform waveguide is known as the Pekeris model.[10] The source is at 13 m depth and 1500-m range from the receiving array. For single receiver transmissions, the receiver is at 10-m depth. Receivers or sensors are added at the depths 9 and 10 m, then 8 and 11 m, etc., to 3 and 17 m.

limit is always 54 Hz and the bandwidth is increased by moving the upper frequency limit only.

The source/receiver geometry within the waveguide is shown schematically in Fig. 2. The source is placed at a depth of 13 m and the hydrophone receivers are spaced 1 m apart on a vertical array 1500 m from the source. When only one receiver is used to filter the signal transmitted by the source, the central hydrophone at 10-m depth is chosen. Additional receivers are incorporated into the filtering process by first adding the hydrophones immediately below and above the 10-m hydrophone (i.e., at 9 and 11 m). Then those at 8 and 12 m are added; and then those at 7 and 13 m, and so on. By this means the length of the receiving array is increased by successive 1-m increments added symmetrically about the central (10-m) point of the water channel. The maximum array length used is 14 m (15 hydrophones).

The transmission from an impulsive source to a receiver is shown in Fig. 3. Figure 3(a) shows the signal for 192-Hz bandwidth and 4 modes (150-Hz center frequency). An increase of the bandwidth to 825 Hz and 13 modes (466.5-Hz center frequency) gives the signal shown in Fig. 3(b). The dispersive transmission in the waveguide causes the impulsive source transmissions to have about 0.15-s duration. Examples of the time-reversed transmissions to matched positions are shown in Fig. 4. The signal bandwidth and the number of modes affect the width of the correlation maxima. Figure 4(a) shows the signal for 192-Hz bandwidth and 4

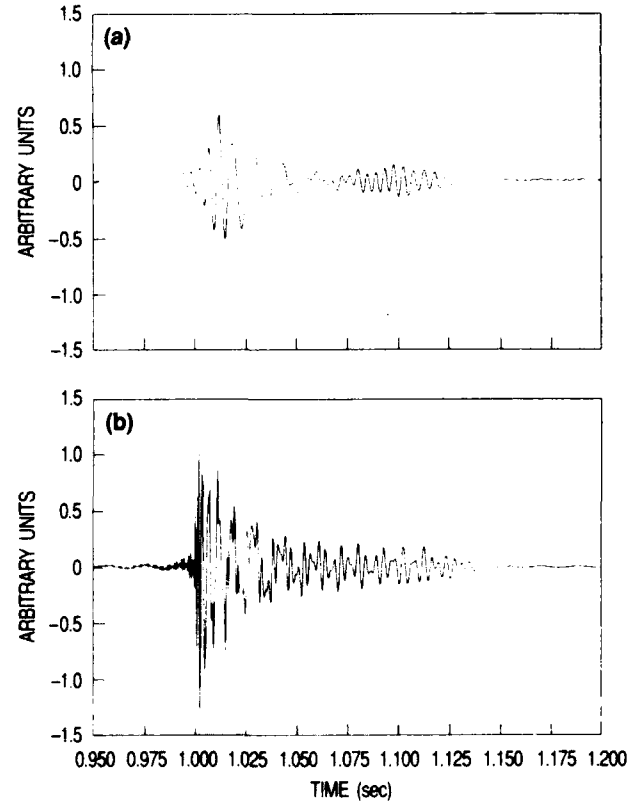

FIG. 3. Transmission from frequency bandlimited source to a single receiver. The geometry and waveguide are shown in Fig. 2. The receiving sensor is at 10-m depth. Compare the complexity of the two examples. (a) Bandwidth 192 Hz and 4 modes. (b) Bandwidth 825 Hz and 13 modes.

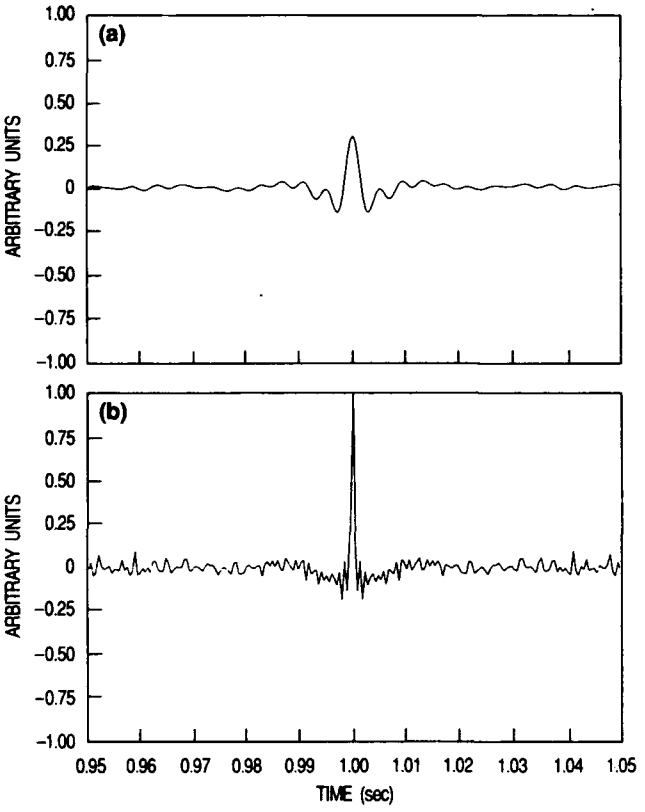

FIG. 4. Time-reversed transmissions to a probe receiver at the source or matched location. The transmissions are from a transducer at 10 m and use all excited modes. (a) Bandwidth 192 Hz and 4 modes. (b) Bandwidth 825 Hz and 13 modes.

modes. An increase of the signal bandwidth to 825 Hz and 13 modes gives the correlation shown in Fig. 4(b). Spatial resolution in source location depends on the reduction of the correlation maximum as the probe receiver is moved away from the matched position. Figure 5 shows the effects of mismatch for the two transmissions shown in Fig. 4. As one would expect, the wide signal bandwidths and more modes show larger effects for mismatch of position. The correlation of the original transmitted signal and the effects of position mismatch were demonstrated a long time ago by Parvulescu and Clay in acoustic transmissions across the Tongue of the Ocean.[11,12,8]

III. MEASURES OF PERFORMANCE, A SIMPLE LOCATOR

Measures of locator performance are functions of signal frequency bandwidth and the number of modes. Performance is also a measure of the spatial resolution and the relative magnitudes of sidelobes as compared to the correlation maximum at the matched position.

A. Sidelobes

A maximum locator, defined as follows, gives a simple measure of relative amplitudes of the sidelobes

$$L_P \equiv \frac{\max|S_p(t_l)|}{\max|S_s(t_k)|}, \tag{18}$$

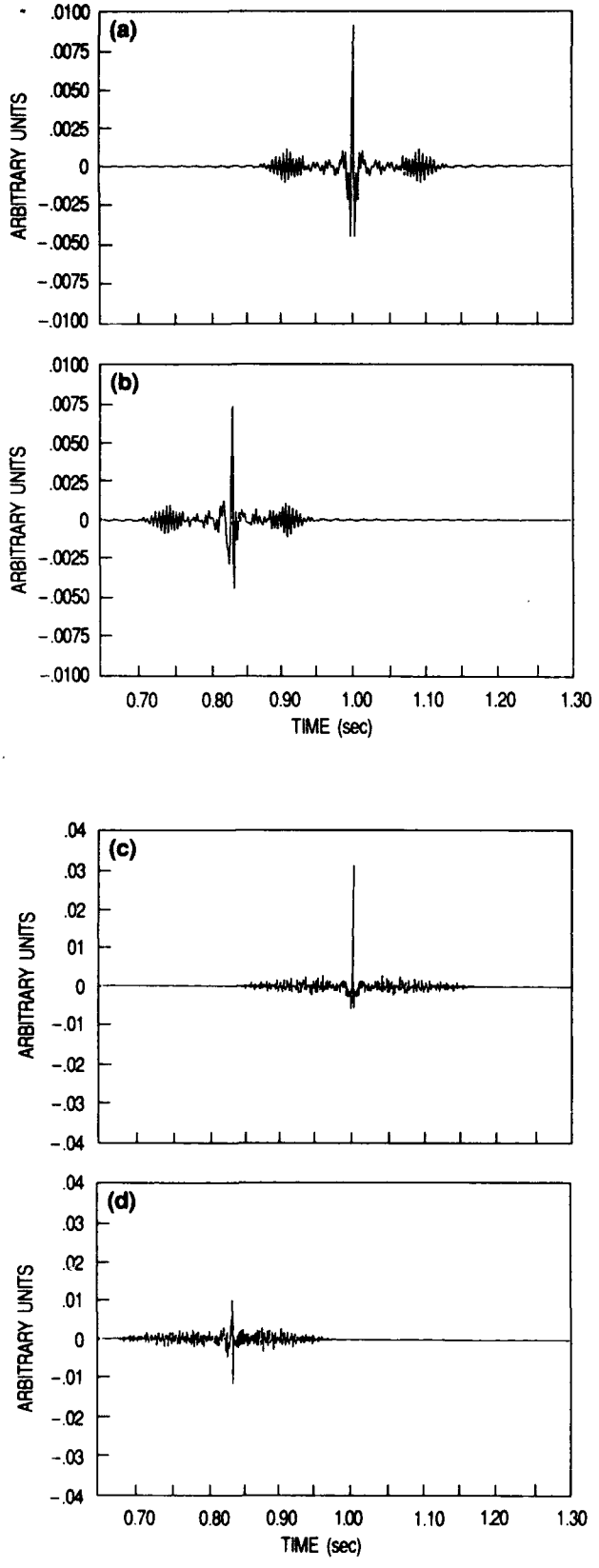

FIG. 5. Time-reversed transmissions to matched and unmatched locations. In all examples the probe receiver depth is $z_p = 13$ m, the same as the original source. The matched range is $r_p = 1500$ m. The unmatched range is $r_p = 1250$ m. (a) Matched position: bandwidth 192 Hz and 4 modes. (b) Unmatched position: bandwidth 192 Hz and 4 modes. (c) Matched position: bandwidth 825 Hz and 13 modes. (d) Unmatched position: bandwidth 825 Hz and 13 modes.

where t_l and t_k are the times of the respective maxima of the probe signal $|S_p(t_l)|$ and the matched signal $|S_s(t_k)|$.

A plot of the relative maxima of the correlations L_p as the probe receiver is moved from the matched position is a simple locator. A typical location curve is shown in Fig. 6. The bandwidth used for this example is 192 Hz. All available propagating modes are used to carry the signal information. This example also uses a full 14-m length, 15-hydrophone array of primary receivers. The source depth is 13 m and the source range is 1500 m from the array.

The curve shown in Fig. 6 clearly indicates a main peak at the correct range. On either side of the main peak, however, are two large sidelobes. We can see that the right-hand sidelobe has a peak-height of ~ 0.95, which makes it a serious ambiguity when attempting to identify and localize the true source. Another major sidelobe appears on the left side of the main peak with height slightly less than 0.9. There are also numerous sidelobes with heights ~ 0.7–0.9.

B. Spatial resolution

Another important aspect of Fig. 6, primarily affecting source localization, is the width of the main signal peak. Ideally we would like to measure this quantity between the 3 dB (i.e., half-height) points on either side of the central maximum. Examination of Fig. 6 shows, however, that the value of the location function does not fall to 0.5 anywhere within

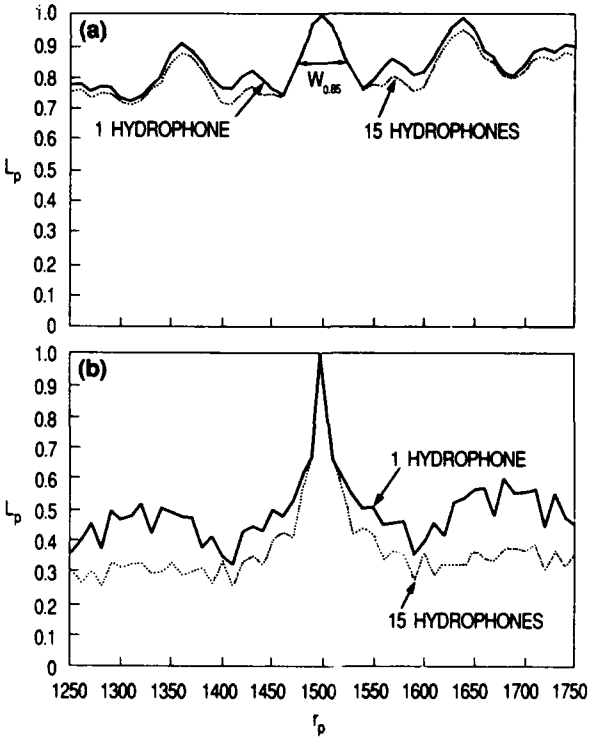

FIG. 6. Locator performance as a function of range to the probe receiver. The locator L_p is defined in Eq. (18). The curves show locator performance as a function of probe range. The probe depth is 13 m, the source depth. The solid curves are for 1 receiver (hydrophone) at 10 m. The dotted curves are for 15 receivers, Fig. 2. The matched position is $r_p = 1500$ m. (a) Bandwidth 192 Hz and 4 modes. (b) Bandwidth 825 Hz and 13 modes.

the range window displayed. This applies not only to this example, but for several other cases considered in this work. In order to be able to quantify the width of the central peak, it was decided to measure the width between points at 0.85 of the maximum value. The two points are indicated in Fig. 6. The curves were drawn by connecting data points, spaced every 12.5 m in range, with a series of short, straight-line segments. The 12.5-m spacing was adopted to reduce the computational cost of doing the problem; but the coarseness of the grid makes accurate measurement of the peak-width difficult. To overcome this difficulty, and allow a reliable and consistent determination of the peak width and peak-to-sidelobe ratio, a 5-point smoothing filter was applied to the location function data for every case. The location function was computed over a much finer grid spacing for comparisons with the smoothed function. Good agreement was observed between the finer grid data and the smoothed function. Both the peak-width measurement and the smoothing procedures were applied identically to the data sets for all cases.

IV. LOCATOR TESTS OF SIGNAL BANDWIDTH, MODES AND ARRAYS

The main peak width and peak-to-sidelobe ratios were obtained and investigated as a function of: (a) frequency bandwidth; (b) number of propagating modes; and (c) number of hydrophone receivers.

A. Frequency bandwidth

Improvements in peak resolution and peak-to-sidelobe ratio, as a result of broadening the frequency bandwidth available for carrying the signal, are based upon the expectation that additional frequency components will add constructively at the (matched) source location and destructively away from the matched location. This should improve the definition of the source peak, by making it narrower and sharper and also reduce the height of sidelobe ambiguities. Figure 4 shows this effect. Increasing the bandwidth of the boxcar source frequency spectrum, from 192 to 825 Hz, significantly sharpens and narrows the correlation maximum.

B. Number of propagating modes

The effect of bandwidth variation upon the acoustic field structure in the waveguide is more complicated than simple frequency addition, because increase of the upper frequency limit also increases the number of propagating modes. The rise and fall of sidelobes is due to the constructive and destructive interference of the normal modes. These are spatially varying and time-varying pressures. Their spatial frequencies, as functions of range, are the horizontal components of the wave numbers. Each frequency component in the source signal will generate its own set of modes (and therefore its own acoustic field) with horizontal wave numbers different from those of the other frequency components. The sum over all frequency components and modes add constructively at the matched location. Away from the matched location, some components will add constructively and others will add destructively. The positions of the sidelobes will vary with frequency. With many frequency components and modes, the sidelobes will tend to small values.

The effect of broadening the bandwidth upon source resolution must be carefully distinguished from that of raising the number of normal modes available to carry the signal information. At higher frequencies the number of normal modes that the waveguide is able to support is greater when a new mode is initiated. This, of itself, will improve the averaging capability for signal enhancement. In this work we want to maintain the distinction between these, and to isolate their individual effects upon the averaging process. In this section we are concerned with increasing the frequency *only*; so we will sometimes encounter the somewhat artificial situation of having a broad frequency band, but deliberately restricting the number of modes below that which the waveguide could support at the high-frequency end of the spectrum. Such a procedure would have a practical application in the use of specially designed arrays to filter and propagate high-frequency signals through the waveguide using only selected modes.

Sidelobes occur where two or more modes interfere constructively at a given range and depth. If modes n and m have horizontal wave numbers κ_n and κ_m, respectively, then the interaction between them is defined by the wave-number difference $\Delta\kappa_{nm} = |\kappa_n - \kappa_m|$. This has an associated interaction distance (or wavelength) $\lambda_{nm} = 2\pi/\Delta\kappa_{nm}$. Sidelobes arising from the interference of modes 1 and 2, for example, will be spaced apart in range by an amount λ_{12} and so on.

In Fig. 7 we see displayed the variation of $\Delta\kappa_{12}$, $\Delta\kappa_{23}$,..., $\Delta\kappa_{89}$, as a function of frequency, for the waveguide under consideration. In the figure we see that the $\Delta\kappa_{12}$ curve starts at a frequency of about 100 Hz (when mode 2 is initiated and available to interfere with mode 1). The $\Delta\kappa_{23}$ starts at about 170 Hz, when mode 3 is initiated, etc. We note that in all the curves displayed the value of $\Delta\kappa$ falls asymptotically from an initial high value to a limit at high frequency which is different for each pair of modes. The improvement in source resolution obtained by frequency averaging is due to the corresponding variation in $\Delta\kappa_{nm}$ for the various pairs of modes

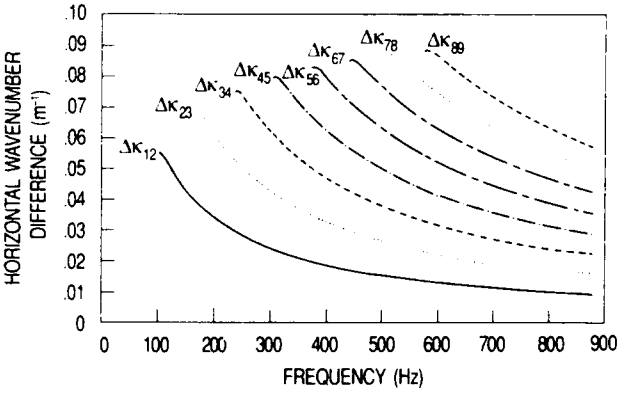

FIG. 7. Horizontal wave-number differences $\Delta\kappa_{n,m}$ as a function of frequency. The differences between wave-number values for pairs of adjacent modes are plotted as a function of frequency. Each curve is plotted from the frequency at which the higher mode of the pair is initiated. For example, the $\Delta\kappa_{12}$ curve begins at a frequency of about 100 Hz, where mode 2 appears.

(n,m) over the frequency range chosen. In Fig. 7 $\Delta\kappa_{12}$, for example, falls from an initial value of about 0.055 m^{-1} at 100 Hz to 0.009 m^{-1} at 878.5 Hz. This corresponds to an increase in the interaction distance λ_{12} from 114 to 698 m over the same bandwidth, which should promote a significant degree of sidelobe suppression.

The effects of insufficient frequency averaging are readily seen in the following example. Figure 8 shows the signal location function for a 192-Hz bandwidth (54–246 Hz) signal, which is emitted from a source placed in the water close to the water/bottom interface (i.e., near 20-m depth) and received by a hydrophone at depth 12 m. The source is placed near to the boundary in order to couple more energy into the higher modes. We see several rapidly varying sidelobes on either side of the signal peak, due primarily to the interaction of modes 1, 2, and 3, which all have significant levels of excitation. Mode 4 is also quite highly excited, but only appears at 238.5 Hz and therefore does not play an important part in the location process over the chosen frequency band. Figure 7 indicates that the average value of $\Delta\kappa_{12}$, over the frequency range in which both modes 1 and 2 are active, is $\approx 3.95\times10^{-2}$ m^{-1}. This corresponds to an average value of $\lambda_{12}\approx 159$ m. Figure 8 clearly shows two sidelobes, one on either side of the signal peak and 160 m from it (labeled "A"). These arise directly from the interaction of modes 1 and 2. The spacing is 160 m, rather than 159 m, because the sampling interval in the data is 10 m. Similarly, the two sidelobes labeled "B" arise from the interaction of modes 2 and 3. The average value of $\Delta\kappa_{23}\approx 5.95\times10^{-2}$ m^{-1}, giving $\lambda_{23}\approx 106$ m. Figure 8 shows the two sidelobes 120 m on either side of the signal peak. This is more than one sampling interval greater than the calculated value; but is still well within the range of values spanned by the data in Fig. 7. The two sidelobes labeled "C" arise from the interaction of modes 1 and 3. The average value of $\Delta\kappa_{13}\approx 9.25\times10^{-2}$ m^{-1}, which gives $\lambda_{13}\approx 68$ m. The "C" sidelobes are 70 m on either side of the signal peak.

The "A," "B," and "C" sidelobes are distinct, sharp and sufficiently close to the signal peak, in both position and peak value, to make accurate identification and localization of the signal difficult. Clearly, the narrow bandwidth used in this example is not sufficient to broaden and reduce the sidelobe level, and thus does not serve to effectively enhance the resolution of the signal peak.

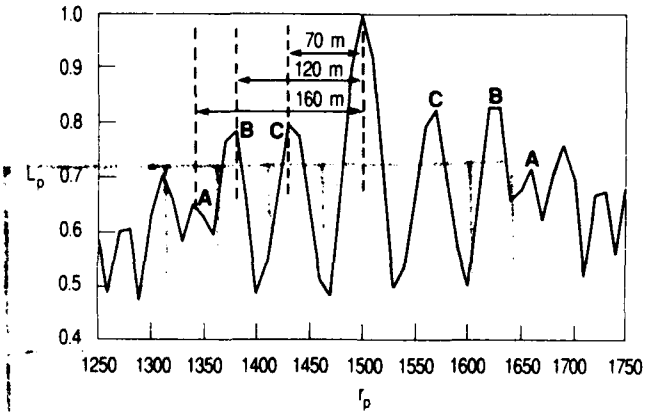

FIG. 8. Locator performance for a source mounted close to the bottom and a single probe receiver. The curve shows locator performance as a function of probe range. The probe depth is 10 m, the source depth is 17 m. The bandwidth is 192 Hz.

C. Arrays

The problem of using more than one receiver in the waveguide is more subtle than it might seem at the outset. By the nature of the solution (1), a sensor at depth z_n senses all modes except the modes for which $\phi_m(z_n)=0$. A sensor at a different depth can sense that mode and increase the information. When all modes are sampled at all frequencies, the addition of more sensors in the array does not appreciably increase the amount of information. Improvement of source location by increasing the number of receivers in an array depends on the number of modes that are propagating and the frequency range.

The performance of the locator defined by (18) has at least two dimensions or measures. The width of the correlation maximum and the relative heights of sidelobes or ambiguities are the more obvious measures. These measures are not orthogonal because the width of the correlation maximum at the matched position and relative sizes of the sidelobes appear to be interrelated. We have chosen to display the width of the correlation maximum at the matched location versus the ratio of the maximum of the sidelobes to the maximum of the correlation at the matched position as predicted by (18). The parametric variables are the frequency bandwidth, number of modes, and number of sensors.

The locator performance for a single receiver is shown in Fig. 9. The variables are the signal bandwidth and the number of modes. The maximum number of modes is limited by the upper frequency limit. Starting on the upper right of the figure the highest frequency is 192 Hz, corresponding to a bandwidth of 138 Hz. Here the performance is poor. As the

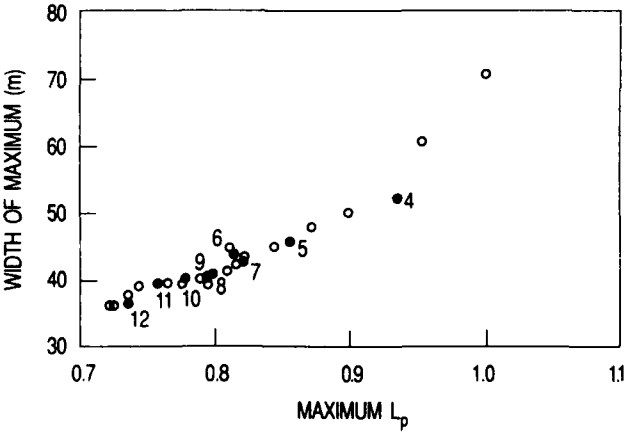

FIG. 9. Locator performance for single receiver and frequency bandwidth. The width of the peak is plotted as a function of maximum sidelobe/peak. The probe receiver depth is 13 m. The sidelobe maximum is for all probe ranges from 1250 to 1750 m. The number of modes increase with increase of the upper frequency limit. The open circle at the upper right is $f=192$ Hz and 4 modes. The next open circle is $f=192+25$ Hz. Solid circles indicate the addition of another mode. Increasing the upper frequency limit moves the circles downward and to the left.

upper frequency limit (and the bandwidth) is increased in 25-Hz increments, the points move downward and to the left. The number of modes also increase as the frequency limit increases. The solid circles and numbers indicate points at which new modes have been added. Although the performance improves as the frequency bandwidth increases, the sidelobe to peak ratio is high, about 0.72 at 842 Hz. The width of the maximum decreases from about 72 to 36 m. The points in Fig. 9 do not fall on a perfectly smooth curve, due to the relatively coarse range sampling interval used to plot the locator function, which was chosen to make the computations tractable. Estimation of the peak width and maximum sidelobe level from the resulting plots [see, for example, Fig. 6(b)] led to small fluctuations in these quantities.

Clearly the signal frequency bandwidth and the number of modes are the primary determinants of locator performance. Our question is how much improvement can we expect by increasing the number of sensors in the array. We have chosen to concentrate on two frequency bands, 192 Hz with 4 modes and 825 Hz with 4 and 12 modes. Referring to Fig. 10, the performance of the locator for 192-Hz signal was poor. The performance of the locator shows the effect of adding sensors to the array. The sidelobe to peak ratio did not change much, but the width of the maximum decreased a little as the number of sensors was increased from 1 to 15. Still keeping only 4 modes, increasing the signal frequency range to 825 Hz put the set of locator performances in a better region. As the number of sensors increased from 1 to 15, the sidelobe-to-peak ratio decreased from about 0.8 to 0.55 and the width decreased from about 50 to 40 m. The same types of computations for all modes gave sidelobe to peak ratios of about 0.73 for 1 sensor and 0.5 for 15 sensors in the array. The widths of the correlation maxima decreased from about 37 to 30 m.

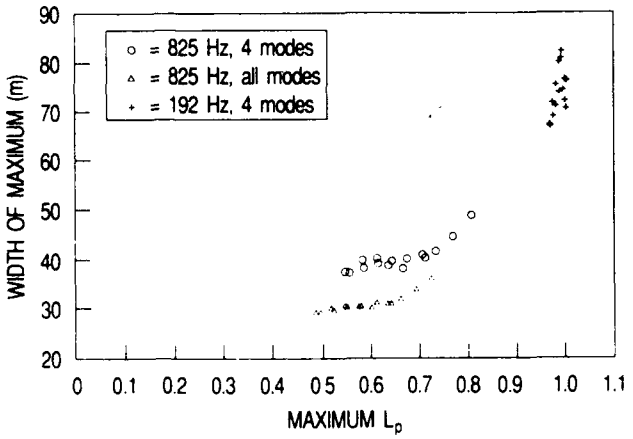

FIG. 10. Locator performance for an array of receivers. Examples are shown for two frequency bandwidths, 192 and 825 Hz. Examples are also shown for 825 Hz with 4 modes and 12 modes. Each of the series of points starts with 1 receiver at the upper left and moves downward and left as the number of receivers in the array increases.

V. CONCLUSIONS

Source location in a simple uniform waveguide is difficult. The sidelobes are large and the correlation maximum is wide. The most effective way to improve locator performance is to increase the signal bandwidth. Increasing the number of modes gives some improvement but no "quantum leaps" occur in either reduction or width of the maximum.

If adequate frequency and mode bandwidths are available, more sensors in the array improve both sidelobe reduction and reduction of the width of the maximum.

ACKNOWLEDGMENT

This work was sponsored by the Naval Research Laboratory 6.1 Program, Element number 61153N (Halcyon E. Morris, Program Manager); and by the Office of Naval Research under Contract N00014-89-J-1515 (CSC). NRL Contribution Number JA 243:034:92.

[1]C. S. Clay, "Optimum time domain signal transmission and source location in a waveguide," J. Acoust Soc. Am. **81**, 660–664 (1987).
[2]S. Li and C. S. Clay, "Optimum time domain signal transmission and source location in a waveguide: Experiments in an ideal wedge waveguide," J. Acoust. Soc. Am. **82**, 1409–1417 (1987).
[3]C. S. Clay and S. Li, "Time domain signal transmission and source location in a waveguide: Matched filter and deconvolution experiments," J. Acoust. Soc. Am. **83**, 1377–1383 (1988).
[4]C. S. Clay, *Elementary Exploration Seismology* (Prentice-Hall, Englewood Cliffs, NJ, 1990), Chaps. 15 and 16.
[5]C. S. Clay, "Use of arrays for acoustic transmission in a noisy ocean," Rev. Geophys. **4**, 475–507 (1966); also in Appendix 6 of Ref. 8.
[6]H. P. Bucker, "Use of calculated sound fields and matched-field detection to locate sound sources in shallow water," J. Acoust. Soc. Am. **59**, 368–373 (1976).
[7]J. Claerbout, *Imaging the Earth's Interior* (Blackwell, Oxford, 1985).
[8]I. Tolstoy and C. S. Clay, *Ocean Acoustics* (American Institute of Physics, New York, 1987), Chap. 4 and Appendix 6.
[9]C. S. Clay and H. Medwin, *Acoustical Oceanography* (Wiley, New York, 1976), Chaps. 9 and A9.
[10]C. L. Pekeris, "Theory of Propagation of Explosive Sound in Shallow Water," Geol. Soc. Am. Mem. **27** (1948).
[11]A. Parvulescu, "Signal detection in a multipath medium by M.E.S.S. processing," J. Acoust. Soc. Am. **33**, 1674 (1961).
[12]A. Parvulescu and C. S. Clay, "Reproducibility of signal transmissions in the ocean," Radio Eng. Electron. **29**, 223–228 (1965).

DTIC QUALITY INSPECTED

Accesion For
NTIS CRA&I
DTIC TAB
Unannounced
Justification
By
Distribution /
Availability Codes
Dist | Avail and / or Special
A-1 | 20